

Entanglement Entropy of Annulus in Three Dimensions

Yuki Nakaguchi^{a,b} and Tatsuma Nishioka^b

^a*Kavli Institute for the Physics and Mathematics of the Universe (WPI)
The University of Tokyo,
5-1-5 Kashiwa-no-Ha, Kashiwa City, Chiba 277-8568, Japan*

^b*Department of Physics, Faculty of Science
The University of Tokyo,
Bunkyo-ku, Tokyo 113-0033, Japan*

E-mail: yuuki.nakaguchi@ipmu.jp,
nishioka@hep-th.phys.s.u-tokyo.ac.jp

ABSTRACT: The entanglement entropy of an annulus is examined in a three-dimensional system with or without a gap. For a free massive scalar field theory, we numerically calculate the mutual information across an annulus. We also study the holographic mutual information in the CGLP background describing a gapped field theory. We discover four types of solutions as the minimal surfaces for the annulus and classify the phase diagrams by varying the inner and outer radii. In both cases, we find the mutual information satisfies the monotonicity dictated by the unitarity and decays exponentially fast as the gap scale is increased. We speculate this is a universal behavior in any gapped system.

Contents

1	Introduction	1
2	Entanglement entropy of annulus	3
2.1	Conformal field theory	4
2.2	A gapped system	5
2.3	Mutual information	6
3	Free massive scalar field	7
3.1	Numerical results	8
3.2	Small and large width limits in CFT	9
4	Holographic entanglement entropy	12
4.1	The AdS ₄ background	13
4.2	The CGLP background	15
5	Universal behaviors	20
A	Details of numerical calculations	23
A.1	Radial lattice discretization	23
A.2	Finite lattice size effect	24
A.3	Large angular momentum	25

1 Introduction

Entanglement entropy is an invaluable tool to explore various aspects of quantum field theories (QFTs) in diverse dimensions, such as critical phenomena [1–8], confinement/deconfinement phase transition [9–13] and renormalization group flow [14–18]. It depends on a state of interest and the shape of an entangling surface Σ that divides a space into a region A and its complement \bar{A} . In the simplest case, Σ is chosen to be a round sphere (or two endpoints of an interval in two dimensions) which allows us to use a conformal transformation [5, 19] and obtain analytic results for conformal field theories (CFTs). Multiple disjoint intervals for CFT₂ are examined by [20–24], and small deformations of an entangling surface in CFT _{$d \geq 3$} are perturbatively studied in

[25–28] recently. More general shapes, however, have not been fully understood so far because of the computational complexity, especially in non-conformal field theories.¹

A special case is a system with a large mass gap where entanglement entropy can be expanded in powers of the inverse of the gap. The coefficients appearing in the expansion are unknown in general, but are assumed to be integrals of the functions of the extrinsic curvature and its derivatives of Σ [31]. The entanglement entropy for Σ diffeomorphic to a circle is examined by [32] for free massive fields in three dimensions, showing that all the coefficients can be systematically determined by the logarithmic divergences of higher-dimensional theories that are the consequence of the conformal anomalies (see also [33]). Similar argument holds for Σ diffeomorphic to multiple disjoint circles.

In this paper, we consider the entanglement entropy of an annulus in QFT_3 as a guide to investigate the phase structure of the ground state.² For CFT, the finite part of the entropy is a function of the ratio of the inner and outer radii $R_1 < R_2$. Unfortunately, the conformal transformation used for a spherical entangling surface [19] does not help us identify the function for the annulus. It, however, was shown in [35] that the strong subadditivity [36] requires the function is concave with respect to $\log(R_2/R_1)$. In a gapped system, the finite part of the entropy depends not only on the ratio, but also on the gap scale, and thus there are no known constraints for the entropy from the strong subadditivity.

To check if the constraints from the strong subadditivity holds for CFT_3 , or more generally to fix the dependence on the ratio and the gapped scale, we perform numerical calculations of the entanglement entropy for a free massive scalar field theory. We put the scalar field on radial lattice following [37] and compute the mutual information across the annulus (see Fig. 2). The mutual information is better than entanglement entropy itself in a sense that it is free from UV divergences and independent of the regularization scheme. For a massless scalar field, the strong subadditivity constrains the mutual information to be a convex function with respect to the ratio of the annulus. We confirm that the convexity holds in our results and inspect the limits of $R_2/R_1 \rightarrow 1$ and $R_2/R_1 \rightarrow \infty$. In the former limit, we approximate the thin annulus by a thin strip (see Fig. 5) and evaluate the mutual information by dimensional reduction to an interval in $(1+1)$ dimensions. In the latter case, we can conformally map the annulus to two disjoint circles whose entanglement entropy is studied both numerically and analytically in the large separation limit [38–40]. We find that our fittings are consistent with the analytic results within our numerical precision. The implementation of the mass is

¹See e.g. [29, 30] for studies on non-conformal theories including finite temperature cases.

²Refer to [34] as a related work on the fuzzy sphere.

straightforward numerically, and we observe that the mutual information exponentially decays as the mass increases while fixing the ratio R_2/R_1 .

Another model we are able to tackle is a strongly coupled QFT holographically dual to the gravity on the AdS space. The holographic calculation of entanglement entropy, known as the Ryu-Takayanagi formula [6, 7, 41], associates the given region A in a QFT_d to a codimension-two minimal surface γ_A satisfying $\partial\gamma_A = \Sigma$ in the AdS_{d+1} space, and gives the entropy S_A by the area of the surface, $S_A = \text{Area}(\gamma_A)/(4G_N)$. It can be applied to disjoint regions and exhibits interesting transitions between different minimal surfaces with the same boundary condition [22], each one of them corresponding to a specific phase in the dual QFT.

We study the holographic entanglement entropy of the annulus by extending the work [32] for a disk in a confining gauge theory with a gap described by the CGLP background [42]. The entropy given by the area of a minimal surface [6, 7] shows a phase transition due to the change of the topology [17]. There are four types of minimal surfaces anchored on the annulus, namely, (1) hemi-torus, (2) two disk, (3) two cylinder, and (4) one disk and one cylinder (disk-cylinder) types. The last three solutions are superpositions of the disk- and cylinder-type solutions found in [32]. The first one was also constructed by [35] in the AdS space. Since the mutual information vanishes for disconnected surfaces only the hemi-torus solution has a non-zero value. Comparing their areas we classify the four phases in the (R_1, R_2) -plane as shown in Fig. 11. The holographic model also exhibits the exponential decay of the mutual information with respect to the gap with the ratio R_2/R_1 fixed.

Based on the observations in the free massive scalar and the holographic models, we speculate that the mutual information through an annulus decays exponentially as

$$I_{\text{annulus}} \sim \exp[-\#m(R_2 - R_1)] , \quad (1.1)$$

in any gapped system with a gap scale m .

2 Entanglement entropy of annulus

In this section, we review general properties of the entanglement entropy for an annulus A in CFT and a gapped system. We discuss its relation to the mutual information between the inner disk and the compliment of the outer disk.

2.1 Conformal field theory

In a three-dimensional CFT, the form of the entropy for an annulus A is fixed by the conformal symmetry,

$$S_A(R_1, R_2) = \alpha \frac{2\pi(R_1 + R_2)}{\epsilon} - f(R_2/R_1) , \quad (2.1)$$

where the first term obeys the area law with the UV cutoff length ϵ and the second term f is a function of the ratio R_2/R_1 of the radii. This function f should be monotonically decreasing and convex

$$f'(\rho) \leq 0 , \quad f''(\rho) \geq 0 , \quad (2.2)$$

with respect to the new variable $\rho = \log(R_2/R_1)$, due to the strong subadditivity

$$S_B + S_C \geq S_{B \cup C} + S_{B \cap C} . \quad (2.3)$$

In what follows, we review the derivation of (2.2) given by [35].

Let the regions B and C be a disk of radius R_2 and an annulus of radii R_1 and R_3 with $R_1 < R_2 < R_3$ as in Fig. 1 (a). The entanglement entropy for a disk of radius R takes a form of

$$S_{\text{disk}}(R) = \alpha \frac{2\pi R}{\epsilon} - F , \quad (2.4)$$

with a constant F .³ The strong subadditivity (2.3) together with (2.1) and (2.4) yields the monotonicity in (2.2):

$$f(R_3/R_1) \leq f(R_2/R_1) . \quad (2.5)$$

The convexity in (2.2) can be derived similarly by taking both B and C as an annulus of radii R_2 and R_4 , and an annulus of radii R_1 and R_3 satisfying $R_1 < R_2 < R_3 < R_4$ as in Fig. 1 (b). In the $R_4 \rightarrow R_3$ limit, the strong subadditivity

$$f(R_4/R_2) + f(R_3/R_1) \leq f(R_4/R_1) + f(R_3/R_2) , \quad (2.6)$$

reduces to the monotonicity of $f'(\rho)$.

³The constant equals to the free energy on S^3 , $F = -\log Z(S^3)$ [19].

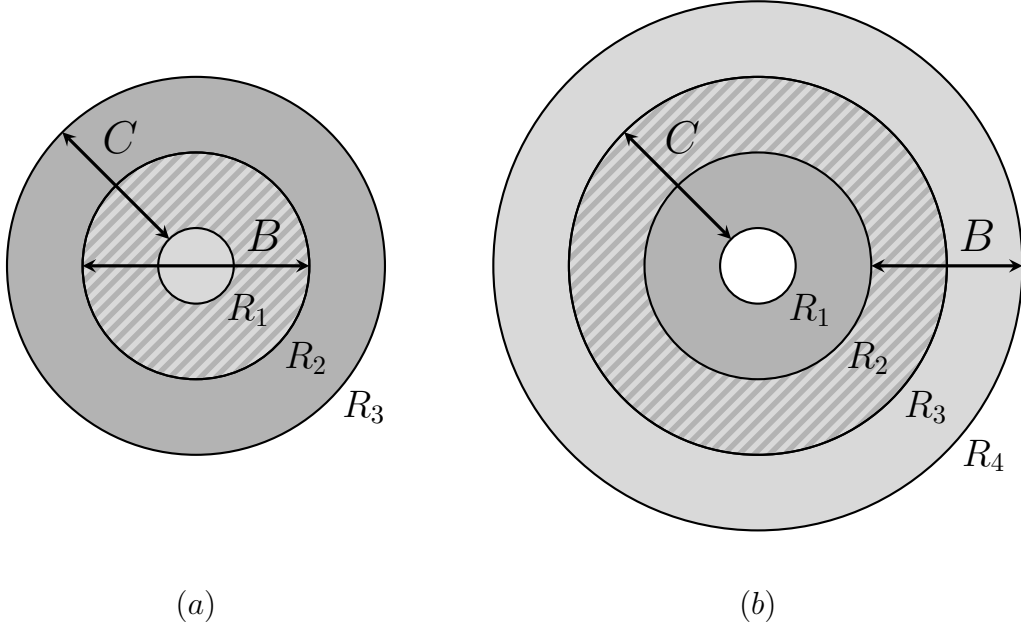


Figure 1. The subsystems B (in light gray) and C (in dark gray) to prove the monotonicity (a) and the convexity (b) of the function f in (2.1). The striped regions are the intersections $B \cap C$.

2.2 A gapped system

In theories with a mass gap of order m , the entanglement entropy of a region A has an expansion in powers of $1/m$:

$$S_A = \alpha \frac{\ell_\Sigma}{\epsilon} + \beta m \ell_\Sigma - \gamma_\Sigma + \sum_{n=0}^{\infty} \frac{c_{2n+1}^\Sigma}{m^{2n+1}}, \quad (2.7)$$

with numerical constants α, β and the topological entanglement entropy γ_Σ [3, 4]. Here the γ_Σ depends on only the topology of the entangling surface $\Sigma = \partial A$ and detects long-range order. The dimensionful coefficients c_{2n+1}^Σ are postulated [31] as local integrals of functions of the extrinsic curvature and its derivatives on Σ . In other words, entanglement contributing to c_{2n+1}^Σ localizes on the entangling surface in the large- m limit due to the short correlation length of order $1/m$.

Applying (2.7) to the annulus A of our interest, the entanglement entropy should take the form of

$$S_A(R_1, R_2, m) = \alpha \frac{2\pi(R_1 + R_2)}{\epsilon} + 2\pi\beta m (R_1 + R_2) - \gamma_\Sigma + \sum_{n=0}^{\infty} \frac{c_{2n+1}^\Sigma}{m^{2n+1}}, \quad (2.8)$$

where Σ is two concentric circles of radii R_1 and R_2 . The coefficients c_{2n+1}^Σ are polynomials of the radii of order $-(2n+1)$.

2.3 Mutual information

The mutual information between two disjoint regions B and C is defined out of the entanglement entropies as

$$I(B, C) \equiv S_B + S_C - S_{B \cup C} . \quad (2.9)$$

It is always finite because the area law divergences cancel by definition, and non-negative because of the subadditivity $S_{B \cup C} \leq S_B + S_C$. In addition, the strong subadditivity yields the monotonicity of the mutual information

$$I(B, C) \leq I(B, C \cup D) , \quad (2.10)$$

for any region D .

To extract the finite parts of the entanglement entropies (2.1) and (2.8) of the annulus A , we take B and C to be two regions outside A , namely, a disk of radius R_1 and the complement of a disk of radius R_2 , respectively (see Fig. 2). We can interpret this mutual information as how much quantum information is shared by B and C across the annulus A . Since the entanglement entropy of a given region is equal to that of the complement, S_C and $S_{B \cup C}$ equal the entropies of a disk of radius R_2 and an annulus of inner and outer radii R_1 and R_2 , respectively. The mutual information I across the annulus A then reduces to

$$I(R_1, R_2) \equiv I(B, C) = S_{\text{disk}}(R_1) + S_{\text{disk}}(R_2) - S_A(R_1, R_2) . \quad (2.11)$$

In this setup, the inequality (2.10) translates into the monotonicity of I with respect to the radii R_1, R_2 :

$$\frac{\partial}{\partial R_1} I(R_1, R_2) \geq 0 , \quad \frac{\partial}{\partial R_2} I(R_1, R_2) \leq 0 , \quad (2.12)$$

which holds for any unitary QFT. The proof proceeds as follows: Let B, C be the regions in Fig. 2 and D be an annulus of radii $R_1 + \Delta R_1$ and R_2 , then the monotonicity $I(B, C) \leq I(B \cup D, C)$ yields $I(R_1, R_2) \leq I(R_1 + \Delta R_1, R_2)$. Similarly let D be an annulus of radii R_1 and $R_2 - \Delta R_2$, then the monotonicity $I(B, C) \leq I(B, C \cup D)$ yields $I(R_1, R_2) \leq I(R_1, R_2 - \Delta R_2)$.

For CFT, the mutual information becomes

$$I_{\text{CFT}} = f(R_2/R_1) - 2F , \quad (2.13)$$

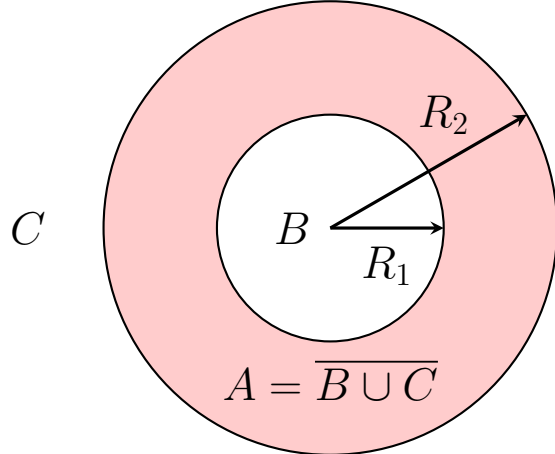


Figure 2. The entangling regions for the mutual information. The region B is a disk of radius R_1 . The region C is the complement of a disk of radius R_2 . The complement of the union of the two regions $\overline{B \cup C}$ is the annulus A in the red colored region.

with the constant F in the disk entropy (2.4), and the inequalities (2.12) are equivalent to the monotonicity of f that was already derived in (2.2).

On the other hand, applying (2.8) for a gapped system to (2.11) leads to

$$I_{\text{gapped}} = \gamma_{\Sigma} - 2\gamma_{\text{disk}} . \quad (2.14)$$

Here the m -dependent terms cancel out due to the assumption that the dimensionful coefficients c_{2n+1}^{Σ} in (2.8) are integrals on the entangling region Σ . Note that the expression (2.14) would fail for small masses such as $mR_1 \lesssim 1$ or $m(R_2 - R_1) \lesssim 1$ if there could exist an exponential term like $O(\exp[-\#m])$ to (2.7) which can not be seen in the large mass expansion. We will discuss such a correction in Section 5.

In the following sections, we will use these mutual informations (2.13) and (2.14) to determine the function f in CFT and to check whether the large mass expansion formula (2.7) holds for the annulus.

3 Free massive scalar field

Let us apply the general discussion on the annulus entropy in Section 2 to a free massive scalar field whose action is defined by

$$I = \frac{1}{2} \int d^3x [(\partial_{\mu}\phi)^2 + m^2\phi^2] . \quad (3.1)$$

In this case, the coefficients β and γ in the entropy (2.8) are known to be $\beta = -1/12$ and $\gamma = 0$.⁴ The coefficients c_{2n+1}^Σ are calculated [32, 33] up to $n = 1$, being local integrals of functions of the extrinsic curvature κ and κ 's derivatives on the Σ . For example,

$$c_1 = -\frac{n_0 + 3n_{1/2}}{480} \int_\Sigma ds \kappa^2 , \quad (3.2)$$

for n_0 free scalar fields and $n_{1/2}$ free Dirac fermions. In the present case, the entangling surface is two disjoint disks of radii R_1, R_2 whose extrinsic curvatures are $\kappa = 1/R_1, 1/R_2$. Thus $c_1^\Sigma = -\frac{\pi}{240}(1/R_1 + 1/R_2)$ for a single free scalar field. The constant term F of the disk entropy (2.4) is analytically calculated as the free energy on a three-sphere, $F_{\text{scalar}} = (\ln 2)/8 - 3\zeta(3)/16\pi^2 \simeq 0.0638$ [43]. The mutual informations (2.13) and (2.14) are

$$I_{\text{massless}} = f(R_2/R_1) - 2F_{\text{scalar}} , \quad (3.3)$$

$$I_{\text{massive}} = 0 . \quad (3.4)$$

3.1 Numerical results

We perform the numerical calculation by putting a free scalar field on the radial lattice following [37, 44], whose details can be found in Appendix A. The main results are presented in Fig. 3 and 4.

Fig. 3 shows the mutual information I (3.3) for the free massless scalar field. The function f satisfies the desired monotonicity and convexity (2.2) with respect to $\rho = \log(R_2/R_1)$ as is clear in Fig. 3 (a). The mutual information I asymptotically vanishes for large R_2/R_1 , which means that the function f has a finite constant term $2F_{\text{scalar}}$. This suggests that the finite constant term is topological and additive for each connected component of the entangling surfaces, namely, proportional to the 0-th Betti number $b_0[\Sigma]$ of Σ . The numerical function $I = I(R_2/R_1)$ is well approximated by $h/(R_2/R_1 - 1)$ with $h \simeq 1/4$ for small width, but h monotonically increases to $h \simeq 1/3$ for large R_2/R_1 (see Fig. 3 (b)). We therefore propose that f is given by

$$f(R_2/R_1) = \frac{h(R_2/R_1)}{R_2/R_1 - 1} + 2F_{\text{scalar}} , \quad (3.5)$$

where $h(R_2/R_1)$ is a mild monotonically increasing function of R_2/R_1 such that $h \simeq 1/4$ for $R_2/R_1 \sim 1$ and $h \simeq 1/3$ for $R_2/R_1 \gg 1$. These asymptotic values are consistent with previous works [40, 45] as will be explained in the next subsections.

⁴The topological entanglement entropy vanishes because there is an empty theory in the IR of the massive scalar theory.

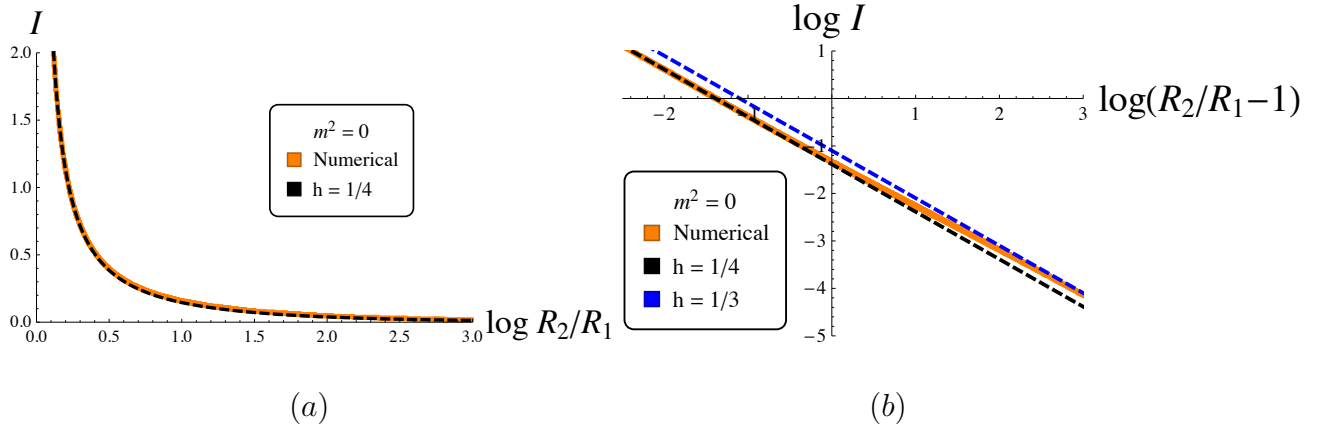


Figure 3. The mutual informations I across the annulus of radii R_1 and R_2 for the free massless scalar field. (a) The mutual information I (the orange line) has the desired monotonicity and convexity, and is well fitted by $h/(R_2/R_1 - 1)$ (the black dotted line). (b) However, this coefficient h is not a constant and increases with R_2/R_1 from $h \simeq 1/4$ (the black dotted line) to $h \simeq 1/3$ (the blue dotted line).

The mutual information (3.3) for the free massive scalar field is displayed in Fig. 4. It is monotonically decreasing with the mass (i.e., decreasing with mR_2 or mR_1 while R_2/R_1 being fixed), and almost vanishes for large mass (Fig. 4 (a)) as is consistent with (3.4). In fact, Fig. 4 (b) demonstrates that the mutual information decays exponentially with a “dimensionless width” $m(R_2 - R_1)$,

$$I_{\text{massive}} \propto m(R_2 + aR_1) \exp[-bm(R_2 - R_1)] , \quad (3.6)$$

with constants a and b . This exponential behaviour satisfies the expected monotonicity (2.12). We will find similar decay even in the holographic model in Section 4 and discuss their possible universality in a gapped phase in Section 5.

3.2 Small and large width limits in CFT

The annulus with small width ($R_2/R_1 \approx 1$) can be approximated by a thin strip of width $R_2 - R_1$ extending along a circle of radius $2\pi R_1$ as in Fig. 5.⁵ The mutual information for the thin strip of width δ is shown to obey [45, 46]

$$I \simeq \kappa \frac{\mathcal{A}}{\delta} , \quad (3.7)$$

⁵We thank T. Takayanagi for drawing our attention to this point.

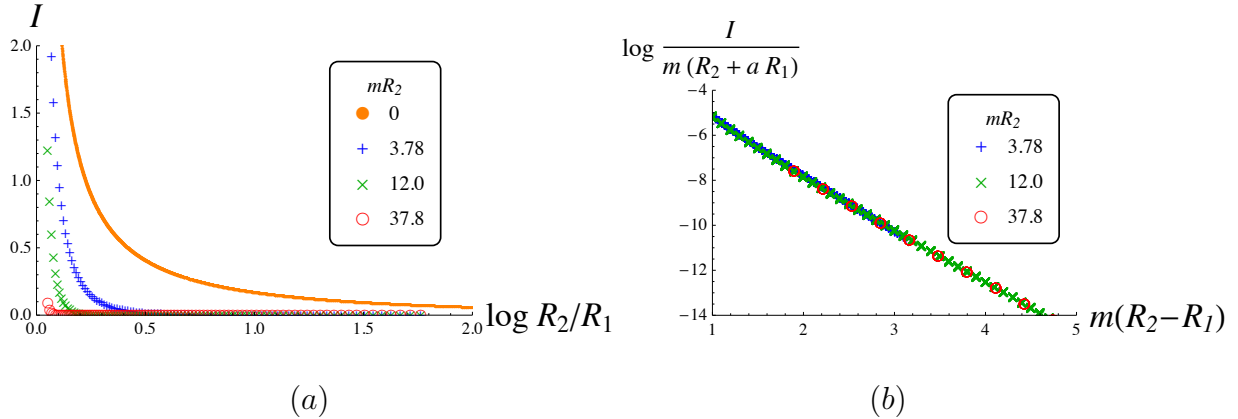


Figure 4. The mutual informations I across the annulus of radii R_1 and R_2 for scalar fields with different masses m . (a) I monotonically decreases with the mass m (orange→blue→green→red). (b) In fact, it exponentially decreases with the dimensionless width $m(R_2 - R_1)$. For $m(R_2 - R_1) \gtrsim 1$, it shows $I \propto m(R_2 + aR_1) \exp[-b m(R_2 - R_1)]$ with $a \simeq 2 \sim 5$ ($a = 3$ in the figure) and $b \simeq 2.5$.

where \mathcal{A} is the area of the plane bounding the strip. This behavior was derived by dimensionally reducing the thin strip to an interval in $(1 + 1)$ dimensions for free fields and summing the mutual informations over the Kaluza-Klein modes.

The coefficient κ is calculated for a free massless scalar field [45] to be $\kappa = 0.0397$. Applying (3.7) to our case, we find

$$I \simeq 0.0397 \frac{2\pi R_1}{R_2 - R_1} = \frac{0.249}{R_2/R_1 - 1}, \quad (3.8)$$

which fits our numerical result in the small width limit ($h \simeq 1/4$ in (3.5)) very well. One may wonder if the small width limit of the mutual information (3.7) is universal and the coefficient κ counts the number of degrees of freedom in any QFT. We will come back to this point in Section 5 where we calculate κ in a holographic model.

Next, consider the opposite limit where the width is large. Let w_i, z_i ($i = 1, 2$) be the two-dimensional Cartesian coordinates related by an inversion transformation

$$(z - z_0)_i = R_T^2 \frac{(w - w_0)_i}{|w - w_0|^2}, \quad (3.9)$$

where w_0 is the inversion point. The inverse map is obtained by exchanging the role of w and z in the transformation with the inversion point at $z = z_0$. R_T is a constant which we can tune arbitrarily.

Consider an annulus in the w -coordinates whose center is at the origin with radii $R_1 < R_2$. Let the points at $w_2 = 0$ on the outer circle be p_1, p_2 and on the inner circle be

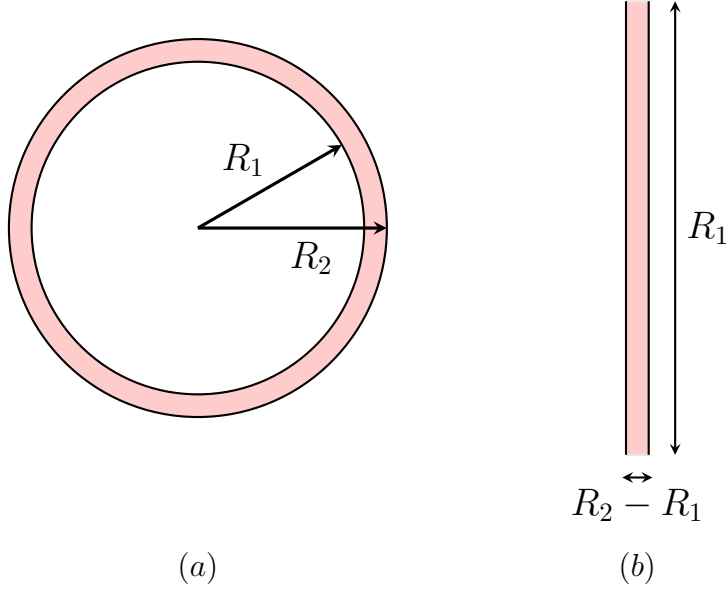


Figure 5. A thin annulus (a) can be approximated by a thin strip (b) with compactified direction.

q_1, q_2 . We choose the inversion points w_0 and z_0 on the real axes at $(w_1, w_2) = (R_0, 0)$ and $(z_1, z_2) = (R'_0, 0)$, respectively. We assume w_0 is inside the annulus, $R_1 < R_0 < R_2$. Under the transformation (3.9), the annulus is mapped to two disjoint circles⁶ (see Fig. 6) and the points p_1, p_2 and q_1, q_2 are at the intersections of the real axis and circles of radii R'_1 and R'_2 given by

$$R'_1 = R_T^2 \frac{R_1}{R_0^2 - R_1^2}, \quad R'_2 = R_T^2 \frac{R_2}{R_2^2 - R_0^2}. \quad (3.10)$$

The distance between the centers of the two circles is

$$r' = R_T^2 R_0 \frac{R_2^2 - R_1^2}{(R_2^2 - R_0^2)(R_0^2 - R_1^2)}. \quad (3.11)$$

The conformal symmetry implies that the cross ratio⁷ x is invariant under the conformal transformation,

$$x = \frac{|p_1 - p_2||q_1 - q_2|}{|p_1 - q_2||p_2 - q_1|}, \quad (3.12)$$

⁶We thank K. Ohmori and Y. Tachikawa for the discussions on this map.

⁷ There are two cross ratios for four points. The other one is

$$y = \frac{|p_1 - p_2||q_1 - q_2|}{|p_1 - q_1||p_2 - q_2|}.$$

which in our case is

$$x = \frac{4R_1R_2}{(R_1 + R_2)^2} = \frac{4R'_1R'_2}{r'^2 - (R'_1 - R'_2)^2} . \quad (3.13)$$

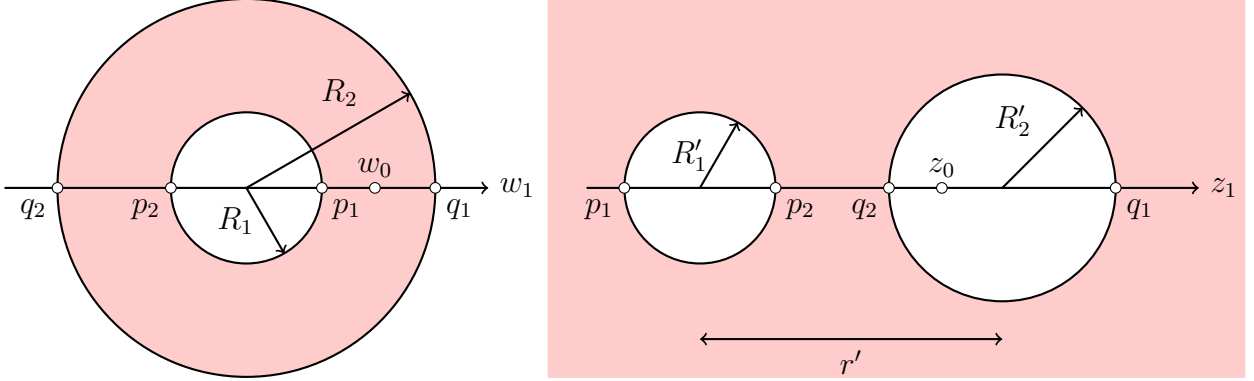


Figure 6. The inversion map of an annulus to two disjoint circles. The region inside the annulus in red color is mapped to the outside of the two circles in red color.

In this way, we can calculate the entanglement entropy of two disjoint circles from that of the corresponding annulus. The former was studied in [38–40] in the widely separated limit for a free massless scalar field. The mutual information between the two circles is [40]

$$I = \frac{1}{3} \frac{R'_1R'_2}{r'^2} + O((R'_1R'_2/r'^2)^2) . \quad (3.14)$$

The inversion maps (3.10) and (3.11) convert it to the mutual information of the annulus,

$$I = \frac{1}{3} \frac{1}{R_2/R_1} + \dots , \quad (3.15)$$

in the large width limit ($R_2/R_1 \gg 1$). What we observed in the previous subsection is nothing but this asymptotic form consistent with numerical result shown in Fig. 3.

4 Holographic entanglement entropy

In this section, we examine the entanglement entropy of an annulus in CFT_3 and a gapped system holographically described by the Einstein-Hilbert gravity in the (asymptotically) AdS_4 space. The holographic formula [6, 7]

$$S_A = \min_{\partial\gamma_A=\Sigma} \frac{\text{Area}[\gamma_A]}{4G_N} , \quad (4.1)$$

associates the entropy of a given region A to the area of a codimension-two minimal surface γ_A homologous to the region A , i.e., $\partial\gamma_A = \Sigma$. Fig. 9 illustrates the cases for A being a disk.

If there are multiple extremal surfaces, we always pick one of them with least area according to the formula (4.1), which yields a transition between minimal surfaces as we vary a parameter such as a gap scale. In this sense, each extremal surface can be regarded as a phase in QFT as we will see in the following.

4.1 The AdS₄ background

We start with CFT₃ dual to the AdS₄ background

$$ds^2 = L^2 \frac{dz^2 - dt^2 + dr^2 + r^2 d\theta^2}{z^2}, \quad (4.2)$$

with the AdS radius L . The original CFT₃ is interpreted to live on the boundary $z = 0$ (or at $z = \epsilon \ll 1$ if UV regularization is needed).

The extremal surface respecting the rotational symmetry of the annulus is a solution to the equation of motion for the action

$$I[r(z)] = \frac{\pi L^2}{2G_N} \int dz \frac{r(z) \sqrt{1 + r'(z)^2}}{z^2}, \quad (4.3)$$

with the boundary conditions $r(0) = R_i$ ($i = 1, 2$) on its ends. There are two possible extremal surfaces depending on their topologies:

- **Two disk phase** (Fig. 7 (2)): γ_A is the superposition of disconnected two disks, each of them being given by

$$r(z) = \sqrt{R_i^2 - z^2}, \quad (i = 1, 2), \quad (4.4)$$

respectively. This solution always exists independent of the size of the annulus.

- **Hemi-torus phase** (Fig. 7 (1)): γ_A is a connected extremal surface. The analytic solution is obtained in the following way [47–49]. It consists of two branches in the (r, z) -plane as

$$r = \begin{cases} R_1 \exp[-f_-(z/r)] , \\ R_2 \exp[-f_+(z/r)] , \end{cases} \quad (4.5)$$

where the functions $f_{\pm}(x)$ are defined using the incomplete elliptic integrals⁸ by

$$f_{\pm}(x) = \frac{1}{2} \log(1+x^2) \pm \eta x_m \left[\mathbb{F}(\omega(x)|\eta^2) - \Pi(1-\eta^2, \omega(x)|\eta^2) \right], \quad (4.7)$$

with the range $0 \leq x \leq x_m \equiv \sqrt{\frac{2\eta^2-1}{1-\eta^2}}$ and $\omega(x) = \arcsin \left[\frac{x/x_m}{\sqrt{1-\eta^2(1-x/x_m)}} \right]$. The parameter η in the range $\eta \in [1/\sqrt{2}, 1]$ is related to the ratio R_2/R_1 of the inner and outer radii of the annulus as

$$\log(R_2/R_1) = 2\eta \sqrt{\frac{2\eta^2-1}{1-\eta^2}} \left[\mathbb{K}(\eta^2) - \Pi(1-\eta^2|\eta^2) \right]. \quad (4.8)$$

This solution is available only for $(1 \leq) R_2/R_1 < 2.724$.

The two disk phase is realized for the large width $R_2/R_1 > 2.724$ where it is the unique solution, while it compete with the hemi-torus phase when $R_2/R_1 < 2.724$. In order to fix the location of the phase transition, we calculate the mutual information I across the annulus defined by (2.11). It is clear in the holographic setup that $I > 0$ signifies the hemi-torus phase because $I = 0$ in the two disk phase.⁹ We benefit from the relevant result of [49] to get the mutual information in the hemi-torus phase¹⁰

$$I_{\text{hemi-torus}} = \frac{\pi L^2}{G_N} \left[\frac{\mathbb{E}(\eta^2) - (1-\eta^2)\mathbb{K}(\eta^2)}{\sqrt{2\eta^2-1}} - 1 \right], \quad (4.10)$$

whose plot is displayed in orange color in Fig. 8. It is a two-valued function whose lower branch is always negative and the upper branch intersects with $I = 0$ at $R_2/R_1 = (R_2/R_1)_{\text{critical}} \approx 2.4$. Since the holographic formula (4.1) selects the non-negative I , the

⁸The definitions of the incomplete elliptic integrals used here are

$$\begin{aligned} \mathbb{F}(x|m) &\equiv \int_0^x d\theta \frac{1}{\sqrt{1-m\sin^2\theta}}, \\ \Pi(n, x|m) &\equiv \int_0^x d\theta \frac{1}{(1-n\sin^2\theta)\sqrt{1-m\sin^2\theta}}, \end{aligned} \quad (4.6)$$

and $\mathbb{K}(m) \equiv \mathbb{F}(\pi/2|m)$ and $\Pi(n|m) \equiv \Pi(n, \pi/2|m)$.

⁹The mutual information can vanish only in the large- N limit and there are $O(1/N)$ corrections [50, 51] for finite N . More generally, the mutual information is bounded from below.

¹⁰The elliptic integral of the second kind is defined by

$$\mathbb{E}(m) \equiv \int_0^{\pi/2} d\theta \sqrt{1-m\sin^2\theta}. \quad (4.9)$$

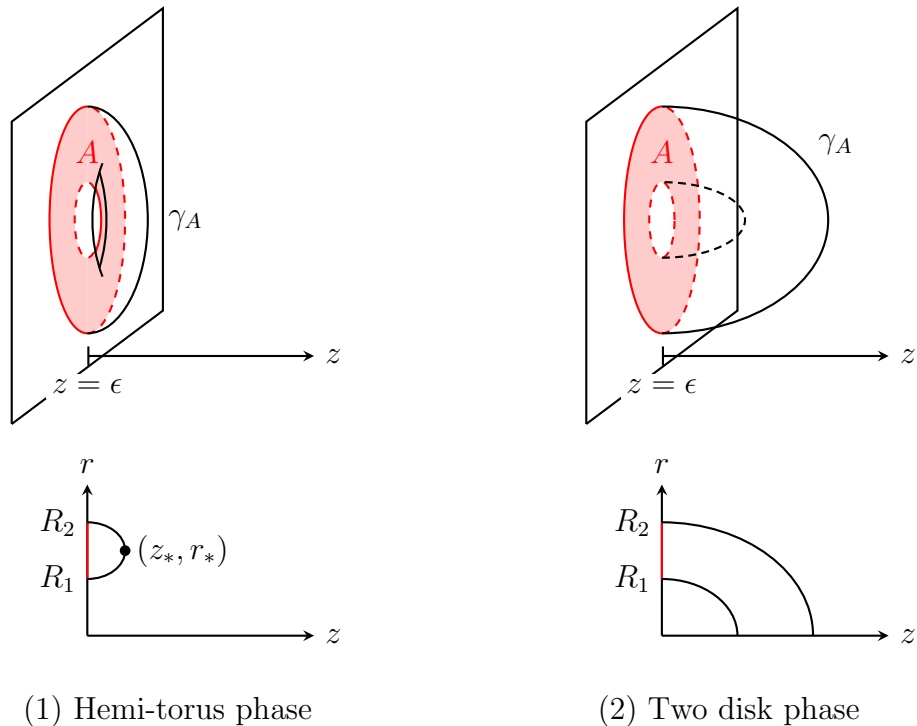


Figure 7. Two phases for the minimal surface in the AdS_4 background: connected hemi-torus phase (1) and disconnected two disk phase (2). Here the time t direction is suppressed.

physical mutual information is given by $I_{\text{hemi-torus}}$ for $R_2/R_1 < (R_2/R_1)_{\text{critical}}$ and $I = 0$ for $(R_2/R_1)_{\text{critical}} < R_2/R_1$. It has a kink at $R_2/R_1 = (R_2/R_1)_{\text{critical}}$ caused by the phase transition of the extremal surface γ_A . Comparing with the general form (2.13) of the mutual information in CFT, Fig. 8 demonstrates the monotonicity and convexity (2.2) of the function f with respect to $\rho = \log(R_2/R_1)$. In other words, the holographic entanglement entropy of an annulus satisfies the strong subadditivity as guaranteed by the holographic proof based on the minimality of the surfaces [52].

4.2 The CGLP background

We move onto a gapped theory described by an asymptotically AdS geometry whose IR region (away from the boundary) is capped off. As a concrete example, we use the CGLP background [42] in M-theory dual to a $(2+1)$ -dimensional QFT with a gap scale.

The CGLP background is a $(3+1)$ -dimensional geometry times a seven-dimensional internal manifold, which asymptotes to the AdS_4 space times the Stiefel manifold $V_{5,2}$.

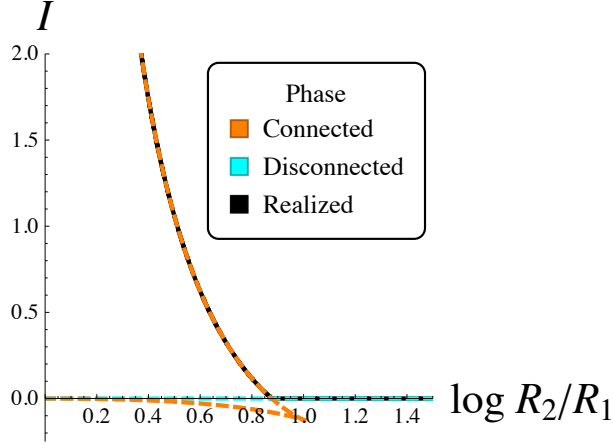


Figure 8. The holographic mutual information I across the annulus of radii R_1 and R_2 for CFT. This mutual information $I = I(R_2/R_1)$ has a phase transition at $(R_2/R_1)_{\text{critical}} \simeq 2.4$, and vanishes for $R_2/R_1 > (R_2/R_1)_{\text{critical}}$ because the disconnected two disk phase is realized.

In the Einstein frame, the metric is given by

$$ds^2 = \alpha(u) [du^2 + \beta(u) (-dt^2 + dr^2 + r^2 d\theta^2)] + g_{ij} dy^i dy^j, \quad (4.11)$$

where u is the holographic coordinate of the AdS_4 ranging from the IR capped-off point 0 to the UV fixed point ∞ . y^i ($i = 1, \dots, 7$) are the coordinates of the internal manifold with a volume

$$V(u) = \int \prod_{i=1}^7 dy^i \sqrt{\det g}, \quad (4.12)$$

vanishing at $u = 0$. The functions in the metric are given by

$$\begin{aligned} \alpha(u) &= \frac{H(u)^{1/3} c^2(u)}{4}, & \beta(u) &= \frac{4}{H(u) c^2(u)}, \\ V(u) &= \frac{3^{17/8} \pi^4 \varepsilon^{21/4}}{2} H^{7/6}(u) (2 + \cosh u)^{3/8} \sinh^{3/2} \left(\frac{u}{2} \right) \sinh^{3/2} u, \\ H(u) &= \frac{L^6}{\varepsilon^{9/2}} 2^{3/2} 3^{11/4} \int_{(2+\cosh u)^{1/4}}^{\infty} \frac{dt}{(t^4 - 1)^{5/2}}, \\ c^2(u) &= \frac{3^{7/4} \varepsilon^{3/2} \cosh^3(u/2)}{2(2 + \cosh u)^{3/4}}, \end{aligned} \quad (4.13)$$

with two dimensionful parameters L and ε . The parameter L is the AdS radius near the boundary, determined by the number of M2-branes N and the Planck length ℓ_p as

$L \equiv 3^{-2/3} 2\pi^{1/3} \ell_p N^{1/6}$. The parameter ε , defining the size of deformation [53], has mass dimension $-4/3$, letting H be dimensionless. V appears to depend on ε , but does not indeed. By rescaling the boundary coordinates (t, r) appropriately, one can remove ε completely from the metric if one wishes.

Let us take a look at the UV behavior of the metric (4.11) for a moment. When u is close to the UV cutoff $u \rightarrow \Lambda \gg 1$, the function $H(u)$ becomes

$$H(u) \rightarrow 2^{15/4} 3^{3/4} L^6 e^{-9u/4} , \quad (4.14)$$

and the other functions approach

$$\begin{aligned} \alpha(u) &\rightarrow \frac{9}{16} L^2 , & \beta(u) &\rightarrow 2^{3/2} 3^{-5/2} L^{-6} e^{3u/2} , \\ V(u) &\rightarrow 3^3 \pi^4 L^{21/2} , & c^2(u) &\rightarrow 2^{-13/4} 3^{7/4} e^{3u/4} . \end{aligned} \quad (4.15)$$

The transformation $z = 2^{5/4} 3^{1/4} L^3 e^{-3u/4}$ takes the metric to the Poincaré coordinates of the AdS_4 space near the boundary

$$ds^2 \rightarrow L^2 \frac{dz^2 - dt^2 + dr^2 + r^2 d\theta^2}{z^2} + \dots . \quad (4.16)$$

Since the extremal surface for a small annulus localizes near the boundary, the entanglement entropy remains to have the previous two phases shown in Fig. 7 in the CGLP background. In addition, there are new phases for a large annulus whose minimal surfaces can reach and terminate on the IR cap-off as we describe below. These are superpositions of disk- and cylinder-type solutions for a disk region [17, 32] depicted in Fig. 9. They have different topologies as the names suggest, and the cylinder-type solution only exists and dominates for a large radius. This resembles the situation for a strip region in a gapped system, which is interpreted as a confinement/deconfinement phase transition [9, 10]. In the present case, the minimal surface switches from the disk-type to the cylinder-type at the critical radius $R = R_{\text{critical}} \simeq 0.72/m$, where $m = \varepsilon^{-3/4}$ is the gap scale determined by the CGLP metric. Taking into account these facts, we end up with three superposed phases; two disk phase, one disk and one cylinder (disk-cylinder) phase, and two cylinder phase. The first one has already appeared for CFT in the previous subsection (see Fig. 7). The second and third ones are drawn in Fig. 10. In total, there are the four phases for the annulus in the CGLP background:

- (1) the hemi-torus phase (Fig. 7 (1)) for $R_2 - R_1 \lesssim 1/m$.
- (2) the two disk phase (Fig. 7 (2)) for $R_1, R_2 < R_{\text{critical}}$,
- (3) the disk-cylinder phase (Fig. 10 (3)) for $R_1 < R_{\text{critical}} < R_2$,

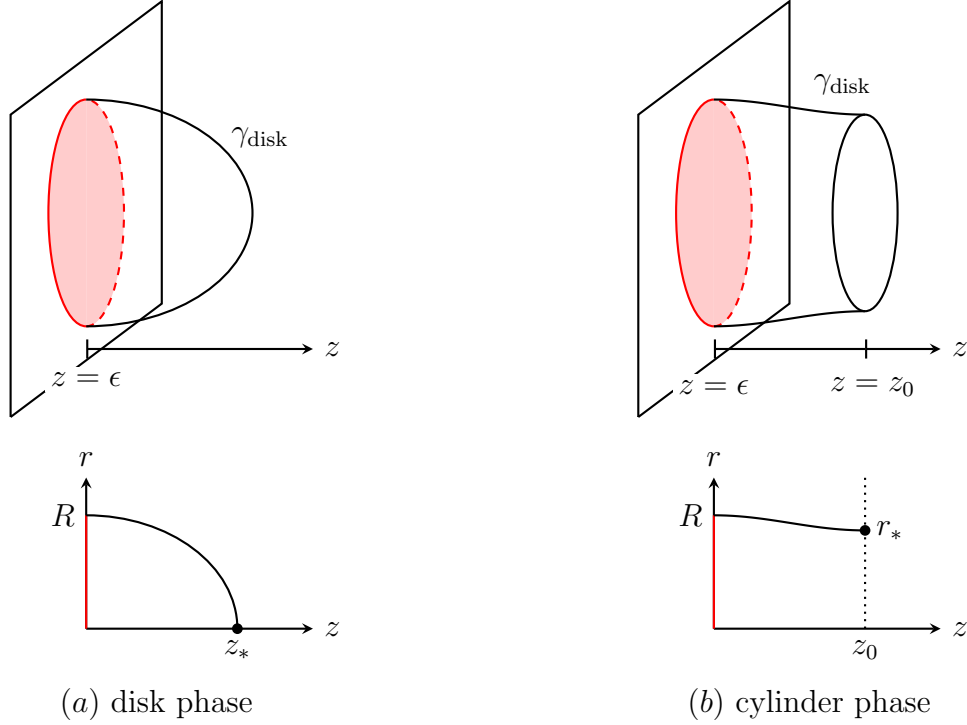


Figure 9. Two phases of the extremal surface in calculating holographic entanglement entropy of disks in the CGLP background: disk phase (a) and cylinder phase (b). In the Poincaré coordinate $z = 2^{5/4} 3^{1/4} L^3 e^{-3u/4}$, the UV boundary $u = \Lambda$ corresponds to $z = \epsilon = 2^{5/4} 3^{1/4} L^3 e^{-3\Lambda/4}$ and the IR capped-off point $u = 0$ corresponds to $z = z_0 = 2^{5/4} 3^{1/4} L^3$. In the cylinder phase, the extremal surface terminates on the IR capped-off point $z = z_0$.

(4) the two cylinder phase (Fig. 10 (4)) for $R_{\text{critical}} < R_1, R_2$,

There are apparently overlaps between the first phase and the others, where the one with the least entropy is realized. To classify the phase structure, we calculate the holographic entanglement entropy in a similar way to the previous pure AdS case. The rotational symmetry lets us assume the radial coordinate r of the extremal surface γ_A as a (two-branched) function $r_{\pm} = r_{\pm}(u)$ of the holographic coordinate u . The area functional becomes

$$I[r(u)] = \frac{\pi}{2G_N} \sum_{\pm} \int du r_{\pm}(u) g(u) \sqrt{1 + \beta(u)(r'_{\pm}(u))^2}, \quad (4.17)$$

with $g(u) = V(u)\alpha(u)\beta^{1/2}(u)$. The extremal surface $r = r(u)$ should satisfy the equa-

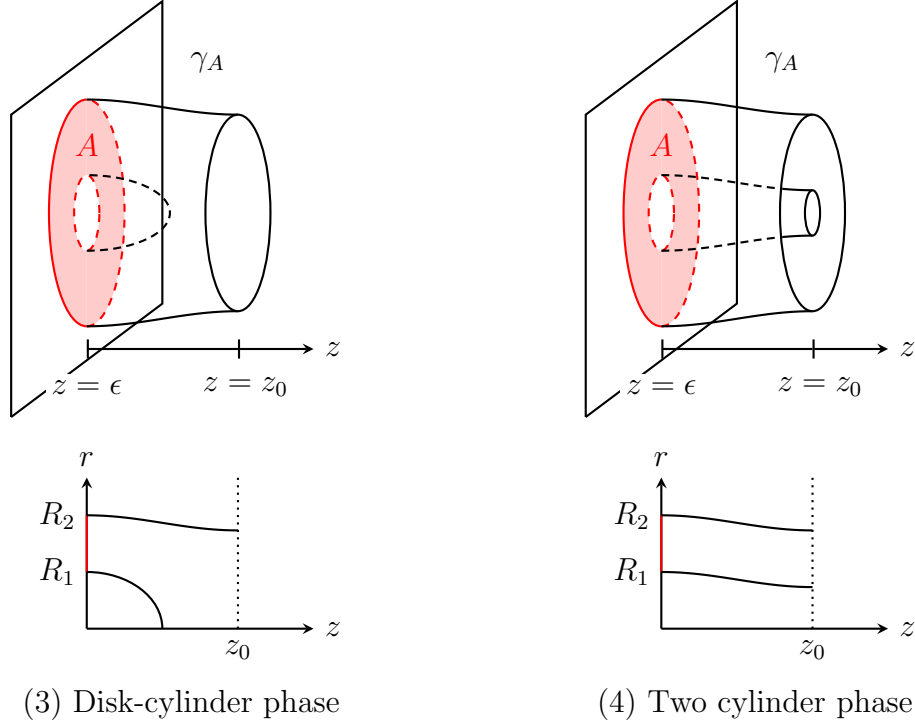


Figure 10. Two new disconnected phases for the minimal surface in the CGLP background: disk-and-cylinder phase (3) and two cylinders phase (4). In the Poincaré coordinate $z = 2^{5/4}3^{1/4}L^3e^{-3u/4}$, the UV boundary $u = \Lambda$ corresponds to $z = \epsilon = 2^{5/4}3^{1/4}L^3e^{-3\Lambda/4}$ and the IR capped-off point $u = 0$ corresponds to $z = z_0 = 2^{5/4}3^{1/4}L^3$.

tion of motion

$$2g(u)\sqrt{1+\beta(u)(r'(u))^2} = \partial_u \left[\frac{r(u)g(u)\beta(u)r'(u)}{\sqrt{1+\beta(u)(r'(u))^2}} \right], \quad (4.18)$$

with the boundary conditions $r_+(\infty) = R_2$ and $r_-(\infty) = R_1$. In contrast to the CFT case, the analytic solution remains to be known. Instead, we employ the numerical calculation by the “shooting method”.

- In the hemi-torus phase, we solve the equation of motion (4.18) from the tip $(r, u) = (r_*, u_*)$ where the two branches meet and have an expansion

$$r_{\pm}(u) = r_* \pm 2\sqrt{\frac{g(u_*)}{g(u_*)\beta'(u_*) + 2g'(u_*)\beta(u_*)}}\sqrt{u - u_*} + O((u - u_*)^{3/2}). \quad (4.19)$$

The radii of the annulus $(R_2, R_1) = (r_+(u = \infty), r_-(u = \infty))$ are functions of (r_*, u_*) , respectively.

- In the three disconnected phases, the extremal surfaces γ_A for the annulus are obtained just by summing the two extremal surfaces $\gamma_{\text{disk}(R_1)}$ and $\gamma_{\text{disk}(R_2)}$ for two disks of radii R_1 and R_2 . The extremal surface $\gamma_{\text{disk}(R)}$ for a disk in the CGLP metric was obtained [32] as follows. The disk-type solution can be constructed by solving the equation of motion (4.18) from the tip of the disk $(r, u) = (0, u_*)$, where the extremal surface shrinks as

$$r(u) = 2\sqrt{\frac{2g(u_*)}{2\beta(u_*)g'(u_*) + g(u_*)\beta(u_*)}}\sqrt{u - u_*} + O((u - u_*)^{3/2}). \quad (4.20)$$

On the other hand, the cylinder-type solution extends to the IR capped-off point $u = 0$ and we solve the equation of motion (4.18) from $(r, u) = (r_*, 0)$ where the extremal surface terminates and behaves as

$$r(u) = r_* + \frac{1}{8r_*\beta(0)}u^2 + O(u^3). \quad (4.21)$$

The disk radius $R = r(\infty)$ is given as a function of u_* or r_* , respectively.

After solving the equation of motion numerically, we compare the holographic entanglement entropies (4.17) between the four phases. The resulting phase diagram is presented in Fig. 11. It shows that the hemi-torus phase is realized when the width of the annulus is small against the gap scale. Note that there is no phase for $R_2/R_1 < 1$ since R_2 is the outer radius of the annulus.

The mutual information (2.11) across the annulus vanishes in all the disconnected phases, and $I > 0$ only in the hemi-torus phase. Fig. 12 shows I as a function of $\log(R_2/R_1)$ with mR_2 fixed. It is positive and decreases as R_2/R_1 becomes large, but vanishes at some point due to the phase transition from the hemi-torus phase to a disconnected phase. It is also monotonically decreasing with the mass for a fixed R_2/R_1 . We will discuss the mass dependence of the mutual information in the next section.

5 Universal behaviors

In the last two sections, we have dealt with the annulus entropies $S_A(R_1, R_2)$ or the mutual informations I across the annulus for the free massive scalar theory and the holographic model. In this section, we will compare these two cases, and attempt to identify universal behaviors of entanglement entropy.

First we consider the small width limit of the mutual information in CFT. From the field theory result, we anticipate (3.7) holds even in the holographic model. Since

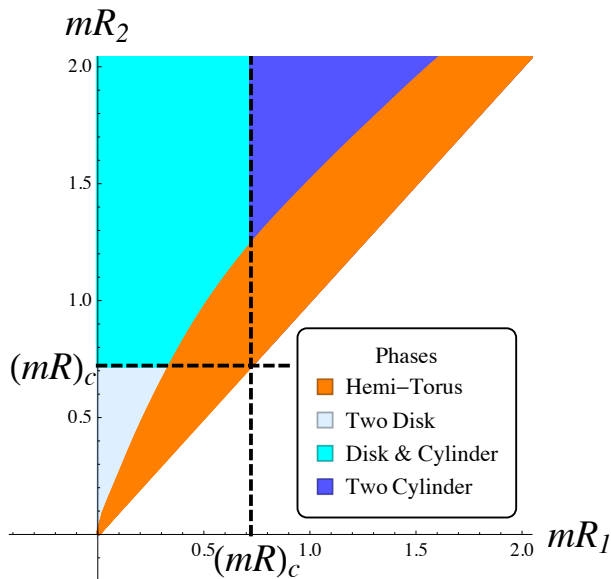


Figure 11. The phase diagram of the entanglement entropy for an annulus of radii R_1 and R_2 . The hemi-torus phase is favored when the width of the annulus is small compared to the gap scale.

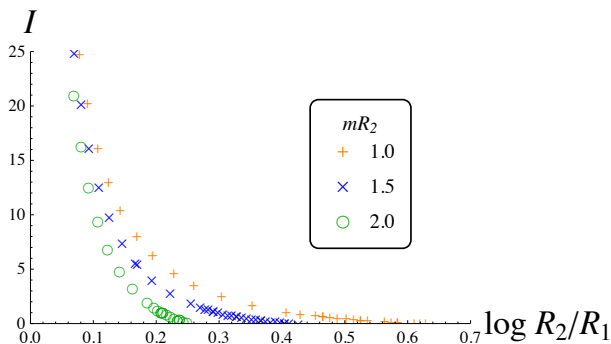


Figure 12. The holographic mutual information I across the annulus of radii R_1 and R_2 in a gapped theory holographically described by CGLP metric. $I = I(mR_1, mR_2)$ vanishes for large R_2/R_1 because the phase becomes disconnected, and monotonically decreases with the mass m increased.

the hemi-torus phase is always favored in the small width limit, we can make use of the relations (4.8) and (4.10). A short calculation yields the small width behavior (3.7)

with the coefficient κ_{hol} given by¹¹

$$\kappa_{\text{hol}} \equiv \frac{L^2 \Gamma[3/4]^4}{2\pi G_N}. \quad (5.1)$$

It is plausible that κ in (3.7) counts the effective degrees of freedom in a given QFT because it is proportional to the number of fields in free field theories which characterize the UV fixed point detected by the small width limit of the mutual information. Indeed, the κ_{hol} in the holographic model decreases under any RG flow thanks to the holographic c -theorem [15, 16, 55, 56] that provides the constraint $L_{\text{UV}} \geq L_{\text{IR}}$ for the AdS radii in the UV and IR fixed points. Similar story may hold for the mutual information through two concentric $(d-2)$ -sphere separated by a short distance δ which behaves as $I \simeq \kappa \text{Area}(S^{d-2})/\delta^{d-2}$ in $d \geq 4$ dimensions [45, 46]. We do not explore this possibility in this paper, but hope to investigate it in the future.

In a gapped system, we observed the exponential decay of the mutual information (3.6) for a free massive scalar field. It provides a strong evidence for the validity of the ansatz (2.7) of the entanglement entropy expanded with respect to the inverse of the gap scale, whose coefficients are the integrals of local invariants localized on the entangling surface. It also implies the existence of an exponentially suppressed correction to the ansatz that will never be seen in the large gap expansion. It is of interest to see to what extent the ansatz (2.7) captures the feature of entanglement entropy in a gapped system. Actually, our holographic calculation in the CGLP background exhibits the exponential decay of the mutual information as in Fig. 13. These observations suggest

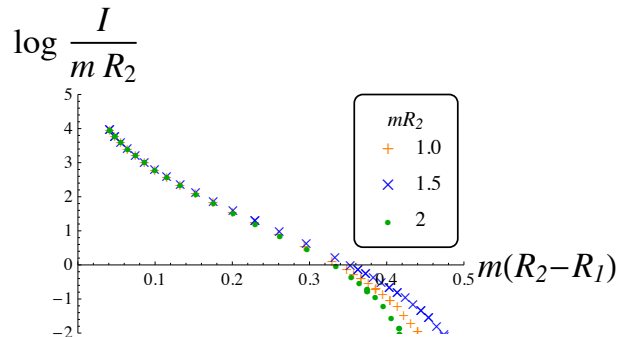


Figure 13. The exponential decay of the holographic mutual information I with the dimensionless width $m(R_2 - R_1)$. For $0.1 \lesssim m(R_2 - R_1) \lesssim 0.3$, it shows $I \propto mR_2 \exp[-b' m(R_2 - R_1)]$ with $b' \simeq 10$. For $m(R_2 - R_1) \gtrsim 0.3$, this exponential behavior ends because of the phase transition to the disconnected phases with $I = 0$.

¹¹ See [54] as a recent related work.

that the entanglement entropy in a system with a gap m has a power series expansion of $1/m$ with an exponential correction

$$S_A = \alpha \frac{\ell_\Sigma}{\epsilon} + \beta m \ell_\Sigma - \gamma_\Sigma + \sum_{n=0}^{\infty} \frac{c_{2n+1}^\Sigma}{m^{2n+1}} + O(\exp[-m\delta]) , \quad (5.2)$$

where δ is proportional to the shortest distance between disjoint entangling surfaces. This is equivalent to the speculation (1.1) for the mutual information of the annulus where $\delta \propto R_2 - R_1$. We conjecture that (5.2) is a universal property in any gapped system. This resembles the universal thermal corrections in entanglement entropy [57–61] and it would be intriguing to find a relationship between them.

Acknowledgments

We are grateful to M. Nozaki, K. Ohmori, N. Shiba, Y. Tachikawa and T. Takayanagi for valuable discussions. The work of Y.N. was supported in part by JSPS Research Fellowship for Young Scientists and World Premier International Research Center Initiative (WPI) from the MEXT of Japan.

A Details of numerical calculations

In this appendix, we summarize the numerical algorithm for calculating the entanglement entropy of the annulus for a free massive scalar field whose action is given by (3.1).

A.1 Radial lattice discretization

We use the polar coordinates to put the theory on the radial lattice

$$ds^2 = -dt^2 + dr^2 + r^2 d\theta^2 . \quad (A.1)$$

The radial coordinate r is discretized to N points with lattice spacing a . After the Fourier decomposition along the angular coordinate θ , the lattice Hamiltonian becomes

$$H = \frac{1}{2} \sum_{n=-\infty}^{\infty} \left[\sum_{i=1}^N \pi_{n,i}^2 + \sum_{i,j=1}^N \phi_{n,i} K_n^{i,j} \phi_{n,j} \right] , \quad (A.2)$$

where $\phi_{n,i}$ and $\pi_{n,i}$ are the discretized scalar field with angular momentum n on the i -th site and its conjugate, respectively. The matrices $K_n^{i,j}$ depend on the angular

momentum and the mass m

$$K_n^{1,1} = \frac{3}{2} + n^2 + (ma)^2, \quad K_n^{i,i} = 2 + \frac{n^2}{i^2} + (ma)^2, \quad K_n^{i,i+1} = K_n^{i+1,i} = -\frac{i+1/2}{\sqrt{i(i+1)}}. \quad (\text{A.3})$$

These are related to the two-point functions of the scalar fields $(X_n)_{ij} = \langle \phi_{n,i} \phi_{n,j} \rangle$ and the momenta $(P_n)_{ij} = \langle \pi_{n,i} \pi_{n,j} \rangle$ as $X_n = \frac{1}{2} K_n^{-1/2}$ and $P_n = \frac{1}{2} K_n^{1/2}$.

The outer and inner radii of the annulus are chosen to be half-integers in units of the lattice spacing, $R_1/a = r_1 + 1/2$ and $R_2/a = r_2 + 1/2$ with integers r_1, r_2 . This choice corresponds to the free boundary condition in the continuum limit. In our calculation, we vary r_2 from 100 to 120 and r_1 from 5 to $r_2 - 5$. The entanglement entropy of the annulus $S(R_1, R_2)$ is obtained by using $(r_2 - r_1) \times (r_2 - r_1)$ submatrices $(X_n^{r_1, r_2})_{ij}$ and $(P_n^{r_1, r_2})_{ij}$ of the correlation functions X_n, P_n with the ranges $r_1 + 1 \leq i, j \leq r_2$ as

$$S(R_1, R_2) = S_0 + 2 \sum_{n=1}^{\infty} S_n, \quad (\text{A.4})$$

where S_n is the contribution from the n -th angular mode

$$S_n = \text{tr} [(C_n + 1/2) \log(C_n + 1/2) - (C_n - 1/2) \log(C_n - 1/2)], \quad (\text{A.5})$$

with $C_n \equiv \sqrt{X_n^{r_1, r_2} P_n^{r_1, r_2}}$. In the following, we describe how to perform this infinite summation over n under controlled numerical errors.

A.2 Finite lattice size effect

To avoid the finite lattice size effect, we repeat the calculation of S_n (A.5) by changing the lattice size N and fit the results $S_n(N)$ with the asymptotic expansion for large N

$$S_n(N) = S_n(\infty) + \sum_{k=1}^{k_{\max}} \frac{a_k}{N^k}. \quad (\text{A.6})$$

We then read off the constant part $S_n(\infty)$ as the value of S_n in the large- N limit. Starting from $N = 200$, we increase the lattice size by $\Delta N = 20$ until the resultant $S_n(\infty)$ stops changing up to error $\delta = 10^{-6}$. We choose the fitting parameter k_{\max} so that the maximum lattice size N is as small as possible. Typically we find $k_{\max} = 3 \sim 10$.

The finite lattice size effect dominates only for small angular momenta n with small masses ma . In our calculation, the maximum lattice size reaches $N \sim 1000$ for $n \lesssim 10$ in the massless case, but $N = 200$ is sufficiently large for $n \gtrsim 20$ or $ma \gtrsim 0.1$. The total numerical error in (A.4) can be estimated to be $O(20\delta) \lesssim O(10^{-4})$.

A.3 Large angular momentum

In the large angular momentum limit $n \rightarrow \infty$, the correlation matrices X_n and P_n approach almost diagonal matrices [32]. The products of the submatrices $X_n^{r_1, r_2} P_n^{r_1, r_2}$ almost equal to $1/4$ times unit matrix up to order $1/n^8$. The nontrivial entries are at the upper-left corners

$$\begin{aligned}
(X_n^{r_1, r_2} P_n^{r_1, r_2})^{r_1+1, r_1+1} &= \frac{1}{4} + \frac{r_1^2(r_1+1)^2}{16n^4} - \frac{r_1^2(r_1+1)^2(2r_1+1)^2(m^2+2)}{32n^6} + O(1/n^8), \\
(X_n^{r_1, r_2} P_n^{r_1, r_2})^{r_1+1, r_1+2} &= \frac{r_1^3(r_1+1)^{3/2}(r_1+2)^{3/2}}{64n^6} + O(1/n^8), \\
(X_n^{r_1, r_2} P_n^{r_1, r_2})^{r_1+2, r_1+1} &= \frac{r_1^2(r_1+2)^{3/2}(r_1-1)^{1/2}(3(r_1+1)^2-1)}{64n^6} + O(1/n^8).
\end{aligned} \tag{A.7}$$

and at the lower-right corners

$$\begin{aligned}
(X_n^{r_1, r_2} P_n^{r_1, r_2})^{r_2, r_2} &= \frac{1}{4} + \frac{r_2^2(r_2+1)^2}{16n^4} - \frac{r_2^2(r_2+1)^2(2r_2+1)^2(m^2+2)}{32n^6} + O(1/n^8), \\
(X_n^{r_1, r_2} P_n^{r_1, r_2})^{r_2, r_2-1} &= \frac{r_2^{3/2}(r_2-1)^{3/2}(r_2+1)^3}{64n^6} + O(1/n^8), \\
(X_n^{r_1, r_2} P_n^{r_1, r_2})^{r_2-1, r_2} &= \frac{r_2^{1/2}(r_2-1)^{3/2}(r_2+1)^2(3r_2^2-1)}{64n^6} + O(1/n^8).
\end{aligned} \tag{A.8}$$

Here we restrict the ranges of r_1, r_2 to $3 \leq r_1$ and $r_1 + 3 < r_2$ to avoid the overlap between the upper-left and lower-right corners, which is satisfied in our set up with $5 \leq r_1 \leq r_2 - 5$.

The $r_2 - r_1 - 2$ eigenvalues of the matrix $\sqrt{X_n^{r_1, r_2} P_n^{r_1, r_2}}$ are $1/2 + O(1/n^8)$ and the other two are given by

$$\frac{1}{2} + c_n^{(a)} - c_n^{(a)} \frac{(2r_a+1)^2(m^2+2)}{2n^2}, \quad c_n^{(a)} \equiv \frac{r_a^2(r_a+1)^2}{16n^4}, \quad a = 1, 2. \tag{A.9}$$

Therefore, most of the eigenvalues do not contribute to the n -th entanglement entropy (A.5) up to order $1/n^8$ and we obtain

$$S_n = \sum_{a=1,2} \left[c_n^{(a)} (1 - \log c_n^{(a)}) + \frac{(2r_a+1)^2(m^2+2)}{2n^2} c_n^{(a)} \log c_n^{(a)} \right] + O(1/n^8). \tag{A.10}$$

This asymptotic formula is much faster than the direct calculation of (A.5).

We perform the matrix trace calculation (A.5) for n less than some large angular momentum n_* , and use this asymptotic formula (A.10) for $n \geq n_*$ as long as $S_n (= O(\log n/n^4))$ is larger than the machine precision. The other higher modes are ignored.

Our n_* is determined as follows. Let the error of $O(1/n^8)$ in (A.10) be μ/n^8 with $\mu = \mu(m, r_1, r_2)$. Then the total numerical error in (A.4) is estimated to be $\sum_{n_*}^{\infty} (\mu/n^8) \sim \mu/(7n_*^7)$. We take n_* to be the angular momentum where the asymptotic formula (A.10) agrees with the matrix trace calculation (A.5) up to $7\delta/n$. Then $\mu/n_*^8 \lesssim 7\delta/n_*$ holds and the total numerical error in (A.4) is bounded by $\sum_{n_*}^{\infty} (\mu/n^8) \sim \mu/(7n_*^7) \lesssim \delta$. In this way, we can handle the numerical error within $O(\delta)$.

References

- [1] C. Holzhey, F. Larsen, and F. Wilczek, *Geometric and Renormalized Entropy in Conformal Field Theory*, *Nucl.Phys.* **B424** (1994) 443–467, [[hep-th/9403108](#)].
- [2] G. Vidal, J. Latorre, E. Rico, and A. Kitaev, *Entanglement in Quantum Critical Phenomena*, *Phys.Rev.Lett.* **90** (2003) 227902, [[quant-ph/0211074](#)].
- [3] A. Kitaev and J. Preskill, *Topological Entanglement Entropy*, *Phys.Rev.Lett.* **96** (2006) 110404, [[hep-th/0510092](#)].
- [4] M. Levin and X.-G. Wen, *Detecting Topological Order in a Ground State Wave Function*, *Phys.Rev.Lett.* **96** (2006) 110405.
- [5] P. Calabrese and J. L. Cardy, *Entanglement Entropy and Quantum Field Theory*, *J. Stat. Mech.* **0406** (2004) P06002, [[hep-th/0405152](#)].
- [6] S. Ryu and T. Takayanagi, *Holographic Derivation of Entanglement Entropy from AdS/CFT*, *Phys.Rev.Lett.* **96** (2006) 181602, [[hep-th/0603001](#)].
- [7] S. Ryu and T. Takayanagi, *Aspects of Holographic Entanglement Entropy*, *JHEP* **0608** (2006) 045, [[hep-th/0605073](#)].
- [8] T. Grover, A. M. Turner, and A. Vishwanath, *Entanglement Entropy of Gapped Phases and Topological Order in Three Dimensions*, *Phys.Rev.* **B84** (2011) 195120, [[arXiv:1108.4038](#)].
- [9] T. Nishioka and T. Takayanagi, *AdS Bubbles, Entropy and Closed String Tachyons*, *JHEP* **0701** (2007) 090, [[hep-th/0611035](#)].
- [10] I. R. Klebanov, D. Kutasov, and A. Murugan, *Entanglement as a Probe of Confinement*, *Nucl. Phys.* **B796** (2008) 274–293, [[arXiv:0709.2140](#)].
- [11] A. Pakman and A. Parnachev, *Topological Entanglement Entropy and Holography*, *JHEP* **07** (2008) 097, [[arXiv:0805.1891](#)].
- [12] P. Buividovich and M. Polikarpov, *Entanglement Entropy in Gauge Theories and the Holographic Principle for Electric Strings*, *Phys.Lett.* **B670** (2008) 141–145, [[arXiv:0806.3376](#)].

- [13] Y. Nakagawa, A. Nakamura, S. Motoki, and V. Zakharov, *Entanglement Entropy of $SU(3)$ Yang-Mills Theory*, *PoS LATA2009* (2009) 188, [[arXiv:0911.2596](#)].
- [14] H. Casini and M. Huerta, *A Finite Entanglement Entropy and the C-Theorem*, *Phys.Lett.* **B600** (2004) 142–150, [[hep-th/0405111](#)].
- [15] R. C. Myers and A. Sinha, *Seeing a C-Theorem with Holography*, *Phys. Rev.* **D82** (2010) 046006, [[arXiv:1006.1263](#)].
- [16] R. C. Myers and A. Sinha, *Holographic C-Theorems in Arbitrary Dimensions*, *JHEP* **1101** (2011) 125, [[arXiv:1011.5819](#)].
- [17] H. Liu and M. Mezei, *A Refinement of Entanglement Entropy and the Number of Degrees of Freedom*, *JHEP* **1304** (2013) 162, [[arXiv:1202.2070](#)].
- [18] H. Casini and M. Huerta, *On the RG Running of the Entanglement Entropy of a Circle*, *Phys.Rev.* **D85** (2012) 125016, [[arXiv:1202.5650](#)].
- [19] H. Casini, M. Huerta, and R. C. Myers, *Towards a Derivation of Holographic Entanglement Entropy*, *JHEP* **1105** (2011) 036, [[arXiv:1102.0440](#)].
- [20] P. Calabrese, J. Cardy, and E. Tonni, *Entanglement Entropy of Two Disjoint Intervals in Conformal Field Theory*, *J.Stat.Mech.* **0911** (2009) P11001, [[arXiv:0905.2069](#)].
- [21] P. Calabrese, J. Cardy, and E. Tonni, *Entanglement Entropy of Two Disjoint Intervals in Conformal Field Theory II*, *J.Stat.Mech.* **1101** (2011) P01021, [[arXiv:1011.5482](#)].
- [22] M. Headrick, *Entanglement Renyi Entropies in Holographic Theories*, *Phys.Rev.* **D82** (2010) 126010, [[arXiv:1006.0047](#)].
- [23] T. Hartman, *Entanglement Entropy at Large Central Charge*, [arXiv:1303.6955](#).
- [24] T. Faulkner, *The Entanglement Renyi Entropies of Disjoint Intervals in AdS/CFT*, [arXiv:1303.7221](#).
- [25] V. Rosenhaus and M. Smolkin, *Entanglement Entropy: a Perturbative Calculation*, [arXiv:1403.3733](#).
- [26] V. Rosenhaus and M. Smolkin, *Entanglement Entropy, Planar Surfaces, and Spectral Functions*, *JHEP* **1409** (2014) 119, [[arXiv:1407.2891](#)].
- [27] A. Allais and M. Mezei, *Some Results on the Shape Dependence of Entanglement and Rényi Entropies*, [arXiv:1407.7249](#).
- [28] A. Lewkowycz and E. Perlmutter, *Universality in the Geometric Dependence of Rényi Entropy*, [arXiv:1407.8171](#).
- [29] O. Ben-Ami, D. Carmi and J. Sonnenschein, *Holographic Entanglement Entropy of Multiple Strips*, *JHEP* **1411** (2014) 144, [[arXiv:1409.6305](#)].
- [30] W. Fischler, A. Kundu and S. Kundu, *Holographic Mutual Information at Finite Temperature*, *Phys. Rev.* **D87** (2013) 126012, [[arXiv:1212.4764](#)].

- [31] T. Grover, A. M. Turner, and A. Vishwanath, *Entanglement entropy of gapped phases and topological order in three dimensions*, *Physical Review B* **84** (2011), no. 19 195120.
- [32] I. R. Klebanov, T. Nishioka, S. S. Pufu, and B. R. Safdi, *On Shape Dependence and RG Flow of Entanglement Entropy*, *JHEP* **1207** (2012) 001, [[arXiv:1204.4160](#)].
- [33] B. R. Safdi, *Exact and Numerical Results on Entanglement Entropy in (5+1)-Dimensional CFT*, *JHEP* **1212** (2012) 005, [[arXiv:1206.5025](#)].
- [34] P. Sabella-Garnier, *Mutual Information on the Fuzzy Sphere*, [arXiv:1409.7069](#).
- [35] T. Hirata and T. Takayanagi, *AdS/CFT and Strong Subadditivity of Entanglement Entropy*, *JHEP* **02** (2007) 042, [[hep-th/0608213](#)].
- [36] E. H. Lieb and M. B. Ruskai, *Proof of the strong subadditivity of quantum-mechanical entropy*, *Journal of Mathematical Physics* **14** (1973), no. 12 1938–1941.
- [37] M. Srednicki, *Entropy and Area*, *Phys.Rev.Lett.* **71** (1993) 666–669, [[hep-th/9303048](#)].
- [38] N. Shiba, *Entanglement Entropy of Two Black Holes and Entanglement Entropic Force*, *Phys.Rev.* **D83** (2011) 065002, [[arXiv:1011.3760](#)].
- [39] N. Shiba, *Entanglement Entropy of Two Spheres*, *JHEP* **1207** (2012) 100, [[arXiv:1201.4865](#)].
- [40] J. Cardy, *Some Results on the Mutual Information of Disjoint Regions in Higher Dimensions*, *J.Phys.* **A46** (2013) 285402, [[arXiv:1304.7985](#)].
- [41] A. Lewkowycz and J. Maldacena, *Generalized Gravitational Entropy*, *JHEP* **1308** (2013) 090, [[arXiv:1304.4926](#)].
- [42] M. Cvetič, G. W. Gibbons, H. Lu, and C. N. Pope, *Ricci-Flat Metrics, Harmonic Forms and Brane Resolutions*, *Commun. Math. Phys.* **232** (2003) 457–500, [[hep-th/0012011](#)].
- [43] I. R. Klebanov, S. S. Pufu, and B. R. Safdi, *F-Theorem without Supersymmetry*, *JHEP* **1110** (2011) 038, [[arXiv:1105.4598](#)].
- [44] M. Huerta, *Numerical Determination of the Entanglement Entropy for Free Fields in the Cylinder*, *Phys.Lett.* **B710** (2012) 691–696, [[arXiv:1112.1277](#)].
- [45] H. Casini and M. Huerta, *Entanglement and Alpha Entropies for a Massive Scalar Field in Two Dimensions*, *J.Stat.Mech.* **0512** (2005) P12012, [[cond-mat/0511014](#)].
- [46] H. Casini and M. Huerta, *Entanglement Entropy in Free Quantum Field Theory*, *J. Phys.* **A42** (2009) 504007, [[arXiv:0905.2562](#)].
- [47] N. Drukker and B. Fiol, *On the Integrability of Wilson Loops in $\text{AdS}_5 \times S^5$: Some Periodic Ansatzes*, *JHEP* **0601** (2006) 056, [[hep-th/0506058](#)].
- [48] A. Dekel and T. Klose, *Correlation Function of Circular Wilson Loops at Strong Coupling*, *JHEP* **1311** (2013) 117, [[arXiv:1309.3203](#)].

- [49] P. Fonda, L. Giomi, A. Salvio, and E. Tonni, *On Shape Dependence of Holographic Mutual Information in AdS₄*, [arXiv:1411.3608](#).
- [50] T. Faulkner, A. Lewkowycz, and J. Maldacena, *Quantum Corrections to Holographic Entanglement Entropy*, *JHEP* **1311** (2013) 074, [[arXiv:1307.2892](#)].
- [51] N. Engelhardt and A. C. Wall, *Quantum Extremal Surfaces: Holographic Entanglement Entropy Beyond the Classical Regime*, [arXiv:1408.3203](#).
- [52] M. Headrick and T. Takayanagi, *A Holographic Proof of the Strong Subadditivity of Entanglement Entropy*, *Phys.Rev.* **D76** (2007) 106013, [[arXiv:0704.3719](#)].
- [53] I. R. Klebanov and S. S. Pufu, *M-Branes and Metastable States*, *JHEP* **08** (2011) 035, [[arXiv:1006.3587](#)].
- [54] C. A. Agon and H. J. Schnitzer, *Holographic Mutual Information at small separations*, [arXiv:1501.0377](#).
- [55] L. Girardello, M. Petrini, M. Porrati, and A. Zaffaroni, *Novel Local CFT and Exact Results on Perturbations of $\mathcal{N} = 4$ Super Yang-Mills from AdS Dynamics*, *JHEP* **12** (1998) 022, [[hep-th/9810126](#)].
- [56] D. Z. Freedman, S. S. Gubser, K. Pilch, and N. P. Warner, *Renormalization Group Flows from Holography Supersymmetry and a C-Theorem*, *Adv. Theor. Math. Phys.* **3** (1999) 363–417, [[hep-th/9904017](#)].
- [57] C. P. Herzog and M. Spillane, *Tracing Through Scalar Entanglement*, *Phys.Rev.* **D87** (2013) 025012, [[arXiv:1209.6368](#)].
- [58] C. P. Herzog and T. Nishioka, *Entanglement Entropy of a Massive Fermion on a Torus*, *JHEP* **1303** (2013) 077, [[arXiv:1301.0336](#)].
- [59] J. Cardy and C. P. Herzog, *Universal Thermal Corrections to Single Interval Entanglement Entropy for Conformal Field Theories*, *Phys.Rev.Lett.* **112** (2014) 171603, [[arXiv:1403.0578](#)].
- [60] C. P. Herzog, *Universal Thermal Corrections to Entanglement Entropy for Conformal Field Theories on Spheres*, *JHEP* **1410** (2014) 28, [[arXiv:1407.1358](#)].
- [61] C. P. Herzog and J. Nian, *Thermal Corrections to Rényi Entropies for Conformal Field Theories*, [arXiv:1411.6505](#).